Development and Kinematic Analysis of Origami-inspired Retractable Roof Structures

Jinyu Lu *, Jiangjun Hou, Ding Lu

School of Civil Engineering, Southeast University, Nanjing 210096, China

Abstract: The application of retractable roof structures has enhanced the urban landscape, particularly in large-scale public buildings. Nevertheless, the utilization of origami mechanisms in such structures has only been explored conceptually, with a lack of practical engineering implementations. In this paper, three novel retractable roof structures, integrating Miura-ori (and its variations) with scissor hinge units, are proposed. We first provide a concise overview of the concepts of Miura-ori (including its arched and fan-shaped variations), scissor joint unit, and plate thickening. Subsequently, coordinated motion conditions for the three proposed retractable roof structures are elaborately derived using geometric formulas, and the corresponding solutions are provided when the coordinated motion is not feasible. Lastly, after parameterizing the thick-plate model, the motion mechanism of the retractable roof structures is analyzed exhaustively. The results indicate that all three new structures can achieve smooth opening and closing operations without motion interference. The proposed novel retractable roof structures enrich the variety of architectural structures and provide practical guidance for engineering applications.

Keywords: Retractable roof structure; Miura-ori; Scissor joint unit; Kinematic analysis

1. Introduction

Although the structure of retractable roofs has a long history, it was not until recent decades that it gained widespread attention and became an essential category of building structures [1–4]. The various forms of retractable roofs not only enrich the urban landscape but also endow new functionalities to building structures.

The retractable roof structure is a type of deployable structure, and as such, its research is closely related to that of truss, plate, and membrane unit systems. The concept of deployable structures was first introduced by American architect Buckminster Fuller in 1960 [5,6]. Inspired by his work, Spanish architect E.P. Pineo proposed a scissor joint unit system that connected two bar members through a central pin joint. This system was first applied to the design of a deployable theater, marking the first use of deployable structures in such a context [7]. Hoberman, based on the scissor joint unit, further developed a unique deployable unit system, which served as the basis for designing a new kind of centrally-symmetric radial retractable roof structure [8].

British scholars You and Pellegrino, building on the research of Hoberman, further expanded the research by developing a new type of fundamental scissor joint unit and constructed a more general deployable structure known as Foldable Bar structure, FBS [9]. Additionally, utilizing the scissor joint unit as the fundamental element, You and Pellegrino, at the same time, proposed a radial retractable structure system [10].

In practice, structural performances, particularly mechanical properties, play a crucial role in the design and analysis of retractable roof structures. Chen and his colleagues [11] conducted a study on the structural performance of deployable planar truss structures and found that the low stiffness of the structure may lead to reduced efficiency in large-span truss structures (due to the significant bending moments to internal forces). To overcome this issue, they proposed adding diagonal bracing and lower chords that are compatible with the original geometry of the scissor joint units, thereby improving the mechanical performance of the structure [11]. Professor Cai [12] has extensively researched various new deployable structures, including angular scissor joint units, folding truss structures, and tensioned cable structures, utilizing theoretical analysis, nonlinear finite element simulations, and physical model experiments. His research focused on the geometric composition, motion process, and mechanical performance of these structures, resulting in a set of highly practical conclusions. In short, a substantial amount of work [3,13,14] has been done on the development, theoretical analysis, and optimization of deployable structures. Nevertheless, there is still a need for further integration and application of these deployable structures in specific engineering areas (for instance, civil engineering) , to fully realize their potential.

Origami has been widely applied in engineering, particularly in deployable structures, due to its diverse configurations. Mechanisms based on the principles of origami are an excellent choice for structures that undergo significant changes in characteristics, such as area, in different states. Origami has been used as a tool for mathematical and scientific research since the end of the 19th century. In the 1990s, research on the mathematics and theory of origami gained popularity in many countries worldwide. De Focatiis et al. [15] used the folding model of the oak leaf as a basis to propose various high-compaction folding methods by connecting several leaf units in different ways, which provided new avenues for the deployable membrane structure. Origami structures have found critical applications in the aerospace field. For instance, a solar panel based on Flasher origami [16], composed of a series of triangles, rectangles, and trapezoids arranged according to specific rules, was developed by the Jet Propulsion Laboratory of NASA, and can be readily deployed into a hexagonal shape. The folding and unfolding ratios of this new structure satisfy the requirement of the aerospace industry for solar panels in both the un- and folded states. Utilizing the unique morphological adaptability of origami, Professor Miura Koryo [17,18], from the Institute of Space and Astronautical Science at the University of Tokyo, invented an origami technique called Miura-ori, which not only saves space but also minimizes losses during the un- and folding processes (reducing the volume of an object by 25 times and increasing its energy density by 14 times). Currently, researchers are exploring the potential of origami techniques in the field of architecture and civil engineering [19–21]. Nevertheless, the application of origami structures in this area, overall, is still relatively limited and primarily focused on temporary structures such as lightweight exhibition halls, galleries, and tents. Expanding the application of origami structures in civil engineering, particularly in large and permanent building structures such as sports stadiums, is a research direction that requires further exploration and development.

We, in this paper, propose a novel retractable roof structure based on origami and conduct an in-depth investigation into its kinematic mechanism, aiming to provide more design options for the first party and foster innovation in building structural design by enabling novel functional and structural possibilities for buildings. We first introduce the geometric principles underlying the Miura-ori, including its arched and fan-shaped variations, and provide an overview of the concepts of rigid origami and the thick plate analysis (Section 2). Further, we utilize scissor joint rectangular units to develop three novel retractable roof structures, derive the compatibility conditions for the coordinated motion of each new retractable roof structure, and propose a corresponding improvement strategy (Section 3). After realizing the deployment of retractable roof structures, a detailed analysis of the structural changes during the motion process is conducted (Section 4). Finally, the conclusion is summarized, while the limitations of the study and the prospects for future research are also described (Section 5).

2. Retractable roof based on the principle of origami mechanism

This section aims to identify suitable origami structures that can be applied to retractable roof structures. Firstly, we elaborate on the fundamental kinematic characteristics of the classic Miura-ori, as well as its arched and fan-shaped variations. Additionally, a detailed introduction is given to the expandable scissor joint unit and its variants. Subsequently, a comprehensive analysis of the thick-plate transformation for the retractable roof is presented. Finally, the parameterization modeling method used in this paper is explained using the classic Miura-ori structure as an example.

2.1 Miura-ori and its variations

The Miura-ori is a classic single-degree-of-freedom origami structure with identical parallelogram-shaped units [17]. The classic Miura-ori, when fully expanded, features longitudinal zigzag creases. Based on the classic Miura-ori, adjusting the longitudinal angle of the zigzag creases to make adjacent longitudinal creases unparallel (with a reasonable angle) while spaced longitudinal creases remain parallel, to get the arched variant of the Miura-ori [22–24]. If the creases that lie along straight lines in the transverse direction are altered to become non-parallel, a different form of Miura-ori, known as the fan-shaped variant, can be achieved [25].

The uniformity of the basic components in the Miura-ori enables us to derive the kinematic behavior of the entire mechanism by just analyzing a single unit. Utilizing the principles of Babuška-Brezzi's spherical trigonometry as well as the constraints governing the mechanism [26–28], more generalized kinematic patterns can be deduced. This approach is further applied to derive the corresponding kinematic patterns for the arched and fan-shaped variants of the Miura-ori.

2.2 Expandable Scissor Joint Unit

We introduce expandable scissor joint units to enhance the strength of the structure and to achieve more convenient control [29,30]. Several scissor joint units, consisting of two bars of equal length hinged together at the center, are connected by hinges at the ends of the bars, which form a rectangular mechanism with a single degree of freedom.

Furthermore, by altering the hinge positions in a single scissor joint unit and satisfying certain conditions, an arched scissor joint unit can also be formed [30]. A novel retractable roof structure can be obtained by combining scissor joint units with deployable grid structures.

2.3 Thick plate retractable roof structures analysis

Rigid origami maintains its shape as a rigid plane throughout the un- and folding process, making it particularly suitable for origami-derived structures with significant thickness [31–33]. We draw inspiration from origami and thick plate theories, and utilize the principles of origami mechanisms to design retractable roof panels. Various thick plate methods, including adjusted the crease position, adjusted the shape, and expanding the gap, etc., have been proposed by different researchers for planar symmetric quadrilateral origami structures [31,32,34–36]. The adjusted shape method is applied in our study to obtain the corresponding thick plates for the retractable roof panels. The calculation formula for the opening ratio of the retractable roof panels is given by Eq. (1) (for a detailed derivation, please refer to Appendix A):

$$\eta = 1 - \sin(\arctan\frac{h}{k}) \tag{1}$$

where η denotes the opening rate, h represents the thickness of the panels being trimmed on both sides of the crease, and k is the length of one side of the symmetrical notches. Furthermore, by visualizing Eq. (1), the variation spectrum of the opening rate can be obtained, as depicted in Fig. 1, which vividly demonstrates the relationship between the variables of plate thickness and notch length with max opening rate.

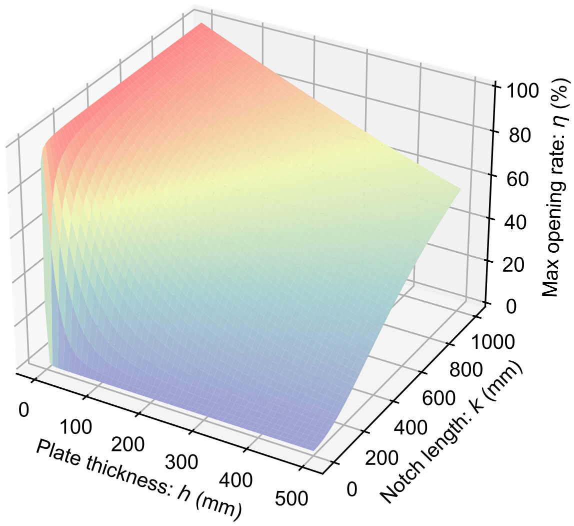

Fig. 1 The variation spectrum of the maximal opening rate.

As shown in Fig. 1, when the notch length is fixed and its value is relatively small, the opening rate decreases with the increase in panel thickness, and the reduction gradually weakens. Meanwhile, when the notch length is fixed and its value is relatively large, the opening rate decreases in a nearly linear manner. Eq. (1), essentially, indicates that the maximum opening ratio is solely determined by the trimmed thickness h and the notch length k, and is irrelevant to factors such as the shape and size of the panel. Therefore, the calculation of the opening rate, for the arched and fan-shaped retractable roof structures, is the same as Eq.(1).

2.4 Parametric modeling of retractable roof structure

Parametric modeling steps using Grasshopper, a powerful parametric modeling software widely used in building structure areas, can be briefly summarized as follows: First, establish a zero-thickness Miura-ori, without considering factors such as the thickness of the panels and the composition of the bars, which is used to determine the shape of the roof unit at different stages of the retractable roof. Then, based on the zero-thickness Miura-ori mechanism, construct a grid structure with thickness. Thereafter, a practical and applicable retractable roof structure is established for specific analysis. A comprehensive guide to the parameterized modeling process can be found in Appendix B.

3. Layout of retractable roof structures

This section further elaborates on the different deployments and forms of the retractable roofs based on the principle of Miura-ori (as well as its arched and fan-shaped variants). First, the deployment of scissor joint units is based on the co-linear and coplanar points that are distributed in a relatively regular manner during the un- and folding process. Geometric formulas are then further employed to validate whether the upper and lower parts of the structure can work synchronously and coordinately. Ultimately, the corresponding optimal methods are proposed for cases where coordinated motion can not be achieved.

3.1 Miura-ori retractable roof

When the Miura-ori mechanism is fully extended, all the mountain and valley vertices of the transverse (span direction, parallel to the x-axis) creases are collinear and located in the same plane（Fig. 2c）. The distances between the mountain and valley vertices in the transverse direction keep unchanged during the deploying process for they share the same basic unit (Fig. 2a). By placing the scissor-jointed rectangular mechanism on the transverse direction of the Miura-ori (the red outline section in Fig. 2c) where the ends of the upper sides of the rectangular mechanism are hinged with the valley vertices of the Miura-ori (Fig. 2e), the motion of these two parts are coordinated in the transverse direction.

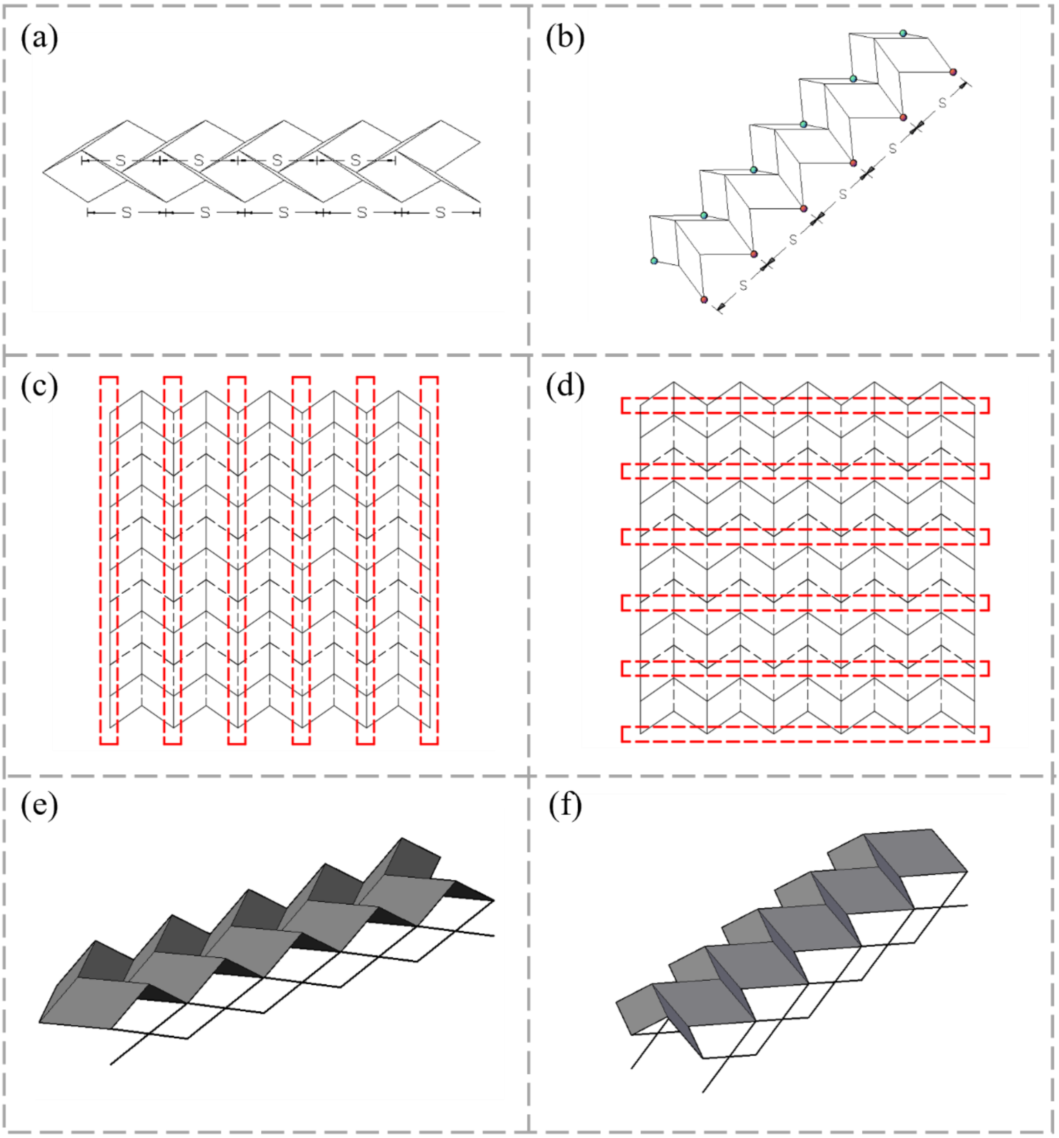

Fig. 2 Miura-ori retractable roof. (a) and (b) denote the transverse and longitudinal origami units, respectively; (c) and (d) depict the location of the transverse and longitudinal scissor joint units; (e) and (f) are the axonometric projection in the transverse and longitudinal direction of scissor joint units.

Similarly, all the vertices of the longitudinal (parallel to the y-axis) creases are collinear throughout the deploying process, and the distances between them remain equal (the distance between the blue dots and the distance between the red dots in Fig. 2b). Additionally, the longitudinally arranged creases, which are spaced apart, remain parallel to each other, and maintain in the same plane during the folding process. By placing the scissor-jointed rectangular mechanism at the inflection point of the longitudinal creases of the Miura-ori, as shown in Fig. 2d, where the upper ends of both sides of the rectangular mechanism are hinged with the vertices of the inflection points of the creases of the Miura-ori (Fig. 2f), the motion of these two parts are coordinated in the longitudinal direction.

The two conditions for the coordinated motion of the scissor-jointed rectangular mechanisms in both x- and y-direction are as follows:

(1) The ratio between the distance of the upper ends of the rectangular mechanism in the x- and y-direction remains constant and is equivalent to the ratio between the distance of the crease vertices of the Miura-ori mechanism in both the x- and y-direction.

(2) The ratio of the relative velocity between the upper ends of the rectangular mechanism in the x- and y-direction is equivalent to the ratio of the relative velocity between the crease vertices of the Miura-ori mechanism in both the x- and y-direction, and it remains constant.

As mentioned above, the distance between the ends of the scissor joint units in both x- and y-direction is always equal to the distance between the corresponding crease vertices. Therefore, the ratio of the distances of the former is equal to the ratio of the distances of the latter, which satisfies condition (1). Nevertheless, for condition (2), further discussion is needed.

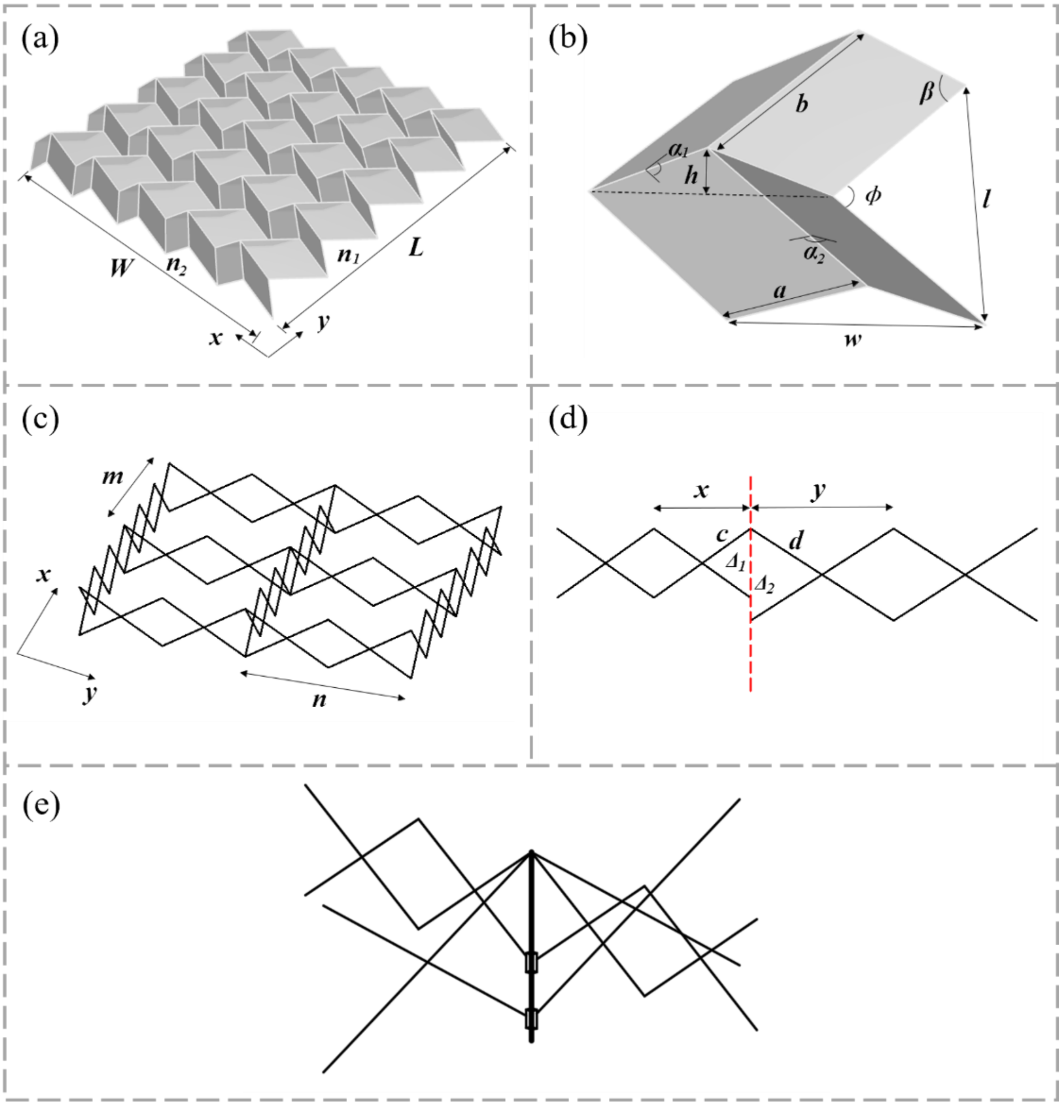

Fig. 3 Geometric parameters of the Miura-ori retractable roof. (a) The overall layout of Miura-ori; (b) Axonometric projection of a panel unit; (c) The overall layout of scissor joint units; (d) Simplified diagram of two scissor joint units; (e) The schematic diagram of the improved scissor joint units. (*W* and *L* represent the length along the x- and y-direction, respectively. n_1 and n_2 represent the number of units in the two directions.)

All the critical geometric parameters of the retractable roof structure, formed by the classic Miura-ori, are diagrammed holistically in Fig. 3. Once the side lengths (a, b) and acute angle (β) of a sub-parallelogram panel unit (Fig. 3b), with four other identical sub-parallelograms, are given, the shape of the basic unit can be determined. The motion of the entire unit is controlled by ϕ, the angle between the two longitudinal creases. According to [37], the length (l), width (w), and height (h) of the basic unit can be expressed as follows:

$$l = 2b\sin(\phi/2) \tag{2}$$

$$w = 2a\frac{\cos\beta}{\cos(\phi/2)} \tag{3}$$

$$h = \frac{a\sqrt{\sin^2\beta - \sin^2(\phi/2)}}{\cos(\phi/2)} \tag{4}$$

The angles formed between the panels of the parallelogram, denoted α_1 and α_2, can be represented as follows:

$$\alpha_1 = \cos^{-1}\left[1 - 2\frac{\sin^2(\phi/2)}{\sin^2\beta}\right] \tag{5}$$

$$\alpha_2 = \cos^{-1}\left[1 - 2\cot^2\beta\tan^2(\phi/2)\right] \tag{6}$$

Fig. 3c-d depicts the three-dimensional scissor joint units mechanism and its essential geometric parameters. To form the whole structure with a single degree of freedom, the scissor joint units require the length of the upper and lower portions of the two scissor joint units at the red dashed line to be equal (Fig. 3d), namely $\Delta_1 = \Delta_2$, which can be expressed as:

$$2\sqrt{c^2 - (\frac{x}{2})^2} = 2\sqrt{d^2 - (\frac{y}{2})^2} \tag{7}$$

where c and d are half of the length of the scissor joint unit in the x- and y-direction, x

and y denote the distance between the upper ends of the scissor joint units in the x- and y-direction, respectively. We, further, formulate the values of x and y using Eqs. (8) and (9):

$$x = \frac{w}{m} = \frac{2a}{m} \cdot \frac{\cos\beta}{\cos(\phi/2)} \tag{8}$$

$$y = \frac{l}{n} = \frac{2b}{n} \cdot \sin(\phi/2) \tag{9}$$

where m and n respectively denote the number of scissor joint units for a single Miura-ori in the x- and y-direction. Substituting the above two equations into Eq. (7) then, we can obtain:

$$\left(\frac{a^2}{m^2}\cos^2\beta\right) \cdot \frac{1}{\cos^2(\phi/2)} - \frac{b^2}{n^2} \cdot \sin^2(\phi/2) = c^2 - d^2 \tag{10}$$

The parameters β, a, b, m, and n above are constants, and the un- and fold of the entire structure is controlled by the parameter φ. Since the left side of the equation is a variable and the right side is a constant, it is not feasible for the three-dimensional scissor joint units connected to the Miura-ori to create a structure with only one degree of freedom. Therefore, an improved design is needed. Fig. 3e is a schematic diagram of the improved scissor joint units. A vertical bar is added to the top of the original scissor joint units to connect with the crease vertex of the Miura-ori. The scissor joint units in both directions are connected at the top, and the bottom ends of the bars are connected to the vertical bar through two sliding joints. In this way, free deploying in the x- and y-direction can be achieved readily, and it is coordinated with the movement of the Miura-ori mechanism at the top.

3.2 Arched variant of retractable roof

In the un- and folding process of the arched variant（Fig. 4a）, the crease vertices at the longitudinal inflection points (parallel to the y-axis) are always collinear. Since the basic units are identical, the distance between the crease vertices in the longitudinal direction (the distance between the blue dots) remains unchanged during the opening and closing process. When arranging the scissor-jointed rectangular mechanism at the longitudinal crease inflection point of the arched variant（the blue outline section in Fig. 4a）, the upper ends of the scissor-jointed units on both sides of the rectangular mechanism are hinged with the crease vertices at the inflection points of the arched variant. Taking only the longitudinal direction, the motion of the upper and lower mechanism is coordinated.

During un- and folding, likewise, the crease vertices along the x-axis are coplanar and the mountain and valley crease vertices in the same plane are located on a single arc segment (red points in Fig. 4a), which creates a uniform distance between the mountain and valley crease vertices in the transverse direction due to the consistent basic units.

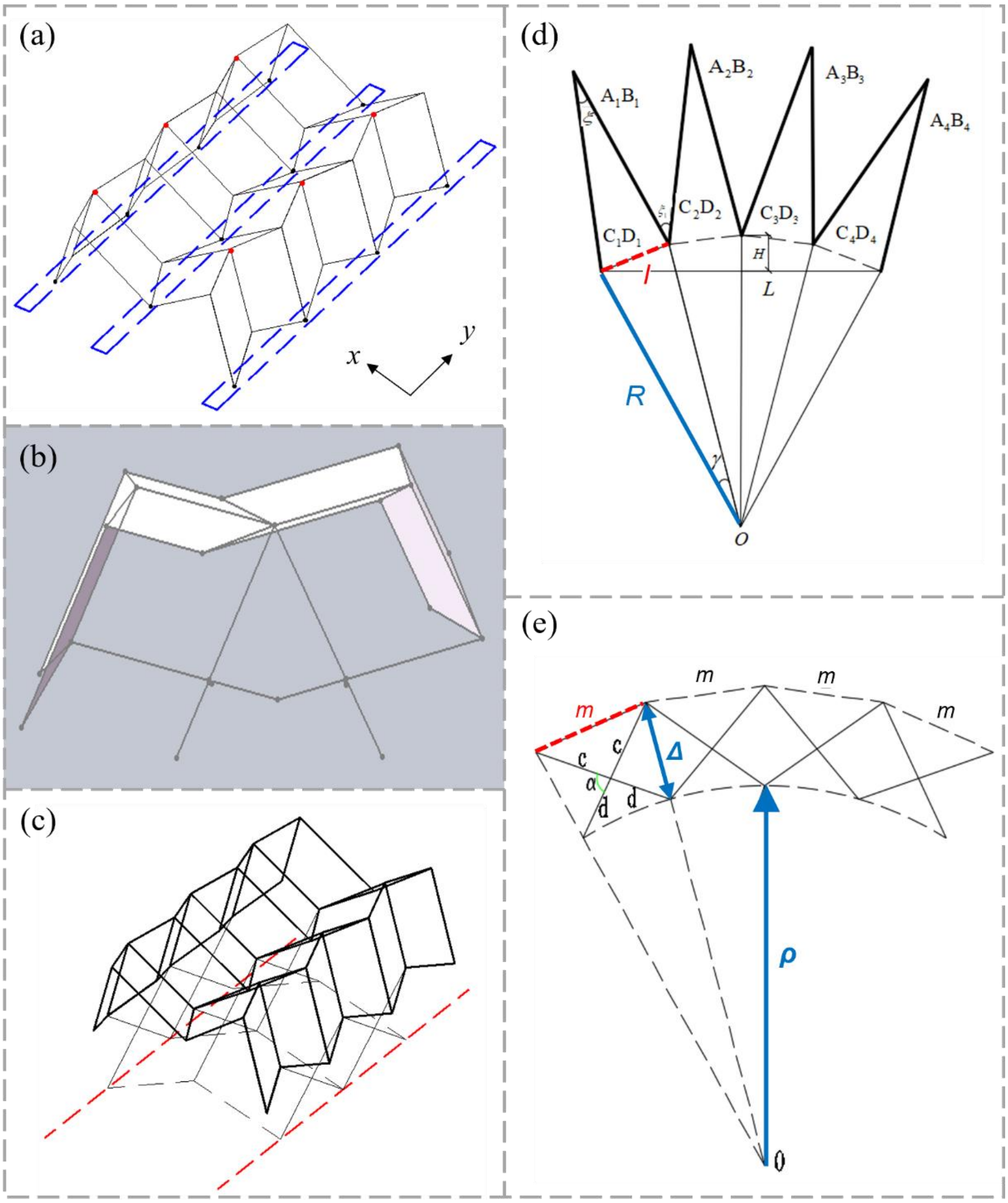

Fig. 4 The arched variant of the retractable roof. (a) The longitudinal distribution of arched variant origami and scissor joint units distribution; (b) The layout of the transverse arched scissor joint unit; (c) The schematic diagram of the improved lower mechanism; (d) Geometric of the upper origami; (e) Geometric parameters of the lower arched scissor joint mechanism.

On the arched variant of the Miura-ori (Fig. 4b), the arched scissor joint units are arranged in a transverse orientation, with the upper portion of the scissor-jointed mechanism hinged to the crease vertices of the arched variant panel. To ensure proper coordination between the scissor-jointed arched mechanism and the upper arched variant of the Miura-ori, two conditions below must be met:

(1) The distance between the ends of the upper bars is equal to the distance between the crease intersections of the upper arched variant of the Miura-ori.

(2) The arc radius between the arched scissor-jointed mechanism and the upper arched variant should maintain consistency throughout the un- and folding process.

Condition (1) necessitates that the distance between the crease intersections at the lower end of the arched variant (denoted as l) must be equal to the distance between the upper bar ends of the arched scissor-jointed mechanism (represented by m), as expressed by Eq. (11) and (12), respectively.

$$l = 2a \cdot \sin\frac{\xi}{2} \tag{11}$$

$$m = 2c\sin(\frac{\pi}{2} - \frac{\alpha}{2}) = 2c\cos\frac{\alpha}{2} \tag{12}$$

In Eq. (11), ξ represents the apex angle of the arched variant (Fig. 4d), while in Eq. (12), α denotes the angle formed between the two bars of the arched scissor-jointed mechanism (Fig. 4e). Condition (1) can be met when α and ξ satisfy Eq. (13):

$$\sin\frac{\xi}{2} = \cos\frac{\alpha}{2} \tag{13}$$

Condition (2) requires that $R = \rho + \Delta$, where R represents the arc radius of the top arched variant of Miura-ori, and $\rho + \Delta$ represents the radius of the upper arc of the arched scissor-jointed mechanism (Fig. 4e). It can be derived from [38] that:

$$\frac{a\cdot\sin\frac{\xi}{2}}{\sin\frac{\xi_1-\xi}{4}}=\frac{\Delta}{r-1}+\Delta=\frac{\sqrt{c^2+d^2-2cd\cos\alpha}}{\frac{c}{d}-1}+\sqrt{c^2+d^2-2cd\cos\alpha} \tag{14}$$

In Eq. (14), introducing a new variable K as shown in Eq. (15), then substituting K into Eq. (14) and conducting simplification, we get Eq. (16).

$$K=\frac{\frac{c}{d}}{a\cdot(\frac{c}{d}-1)}=\frac{c}{ac-ad} \tag{15}$$

$$\frac{\sin^2\frac{\xi}{2}}{\sin^2(\frac{\xi_1-\xi}{4})}+2cd\cos\alpha=K^2\cdot(c^2+d^2) \tag{16}$$

Eq. (16) features the constants a, c, and d, making K a constant. The un- and folding of the entire mechanism are regulated by ξ, ξ_1, and α. The right side of the equation is a constant, while the left side is indeterminate, which suggests that the three-dimensional scissor-jointed units, linked to the arched variant of the Miura-ori, cannot create a mechanism with a single degree of freedom.

We present an enhanced design for the arched variant of the Miura-ori, depicted in Fig. 4c, in which the longitudinal arrangement remains unaltered, but the arched scissor-jointed units in the transverse direction are substituted with prestressed steel cables (or telescopic bars). This modification facilitates unrestricted un- and folding in both the x- and y-direction, while guaranteeing the coordinated motion of the lower arched scissor-jointed mechanism and the upper arched variant of the Miura-ori.

3.3 Fan-shaped variant of retractable roof

During the un- and folding of the fan-shaped variant mechanism, the crease vertices in the radial direction remain coplanar, while within the same plane, all mountain crease vertices and valley crease vertices are collinear. The geometric properties of the fan-shaped variant in the transverse direction make it convenient to arrange the scissor-jointed mechanism. The distances between the mountain crease vertices (represented in red) and valley crease vertices (shown in blue) in the radial direction remain constant during the folding process, by virtue of the identical basic units (Fig. 5a). As a result, arched scissor joint units similar to those used in the longitudinal direction can be utilized in the radial direction, allowing for the hinging and assembly of the upper structure (Fig. 5b).

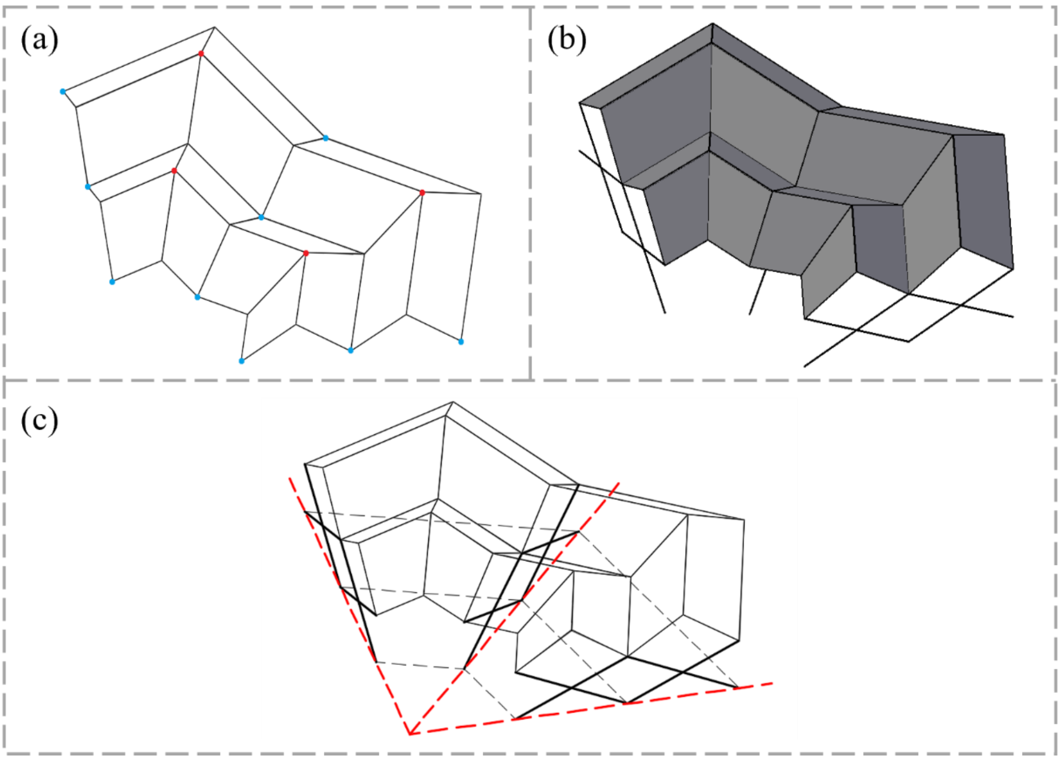

Fig. 5 The fan-shaped variant of the retractable roof. (a) The layout of the origami; (b) The arrangement of the scissor joint units; (c) The schematic diagram of the improved fan-shaped variation.

Similarly, additional prestressed steel cables or rotatable tracks (Fig. 5c) can be added between the lower bar ends of adjacent scissor-jointed rectangular units in the radial direction, which not only ensures coordination with the upper fan-shaped variant mechanism, but also helps to improve the overall integrity and stability of the structure.

4. Motion simulation of retractable roof based on origami principles

In this section, the structure models of the retractable roof structures based on origami principles are simplified, and then SolidWorks, a three-dimensional simulation software, is adopted to simulate its motion. After verifying that the roof panel with thickness can un- and fold smoothly, the variation law of the structure during its motion is analyzed. The kinematic analysis of the three new retractable forms is investigated exhaustively.

4.1 Miura-ori retractable roof

We assume that, as shown in Fig. 6, the Miura-ori retractable roof model consists of four basic units, with two units longitudinally and transversely each. The length of each bar in the lower scissor joint unit is $2c$ = 3100 mm and $2d$ = 3570 mm.

Considering the thickness of the upper roof panel and the dimensions of the lower scissor hinge on the structural motion, two angles, namely ϕ_1 = 20° and ϕ_2 = 120°, which correspond to the fully folded and unfolded states, respectively, are adopted to prevent interference phenomena. Throughout the entire opening and closing process, the angular variation between the roof panels totals 100°. Detailed parameters of the model are presented in Table 1.

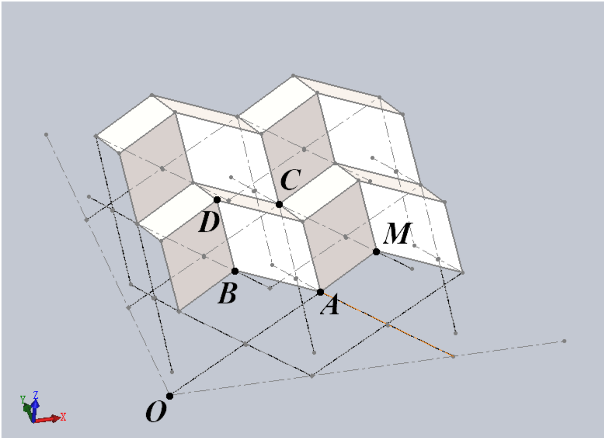

Fig. 6 Miura-ori retractable roof model. A, B, C, and D denote reference points; point O represents the motion center of the structure; point M denotes the place where the rotational driving motor is set.

Table 1 The detailed parameters of Miura-ori retractable roof

a (mm)	b (mm)	β (°)	ϕ_1 (°)	ϕ_2 (°)	c (mm)	d (mm)
1500	1732	60	20	120	1550	1785

Note: the parameters are illustrated in Fig. 3.

To simulate the motion of adjacent roof panels rotating 100 degrees using SolidWorks, we incorporated a rotational driving motor at point M, the intersection of the bottom edges of the two panels, as illustrated in Fig. 6. The angle between the panels increases uniformly at a constant angular velocity of 10 °/s for 10 seconds. Our simulation, depicted in Fig. 7, demonstrates that the whole mechanism can successfully un- and fold as an entirety.

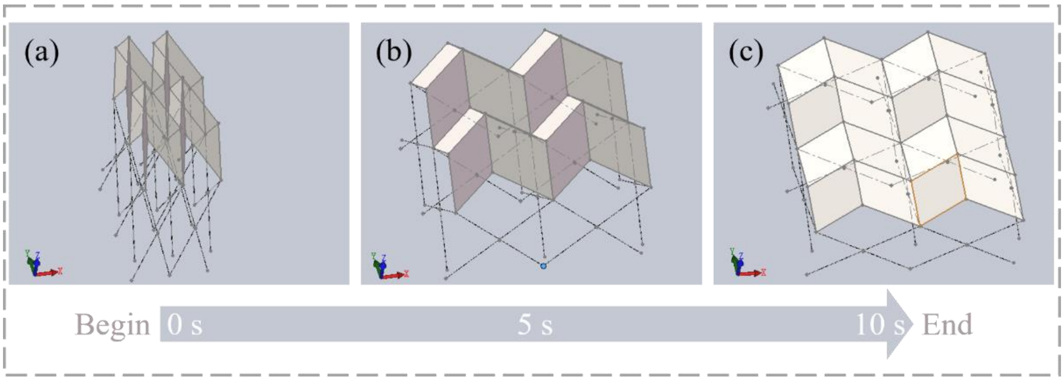

Fig. 7 The motion of the Miura-ori retractable roof. (a), (b), and (c) respectively denote the 0th, 5th, and 10th seconds during the course of motion.

The displacement-time curves of reference points A, B, C, and D relative to the center point O of the orbit are illustrated in Fig. 8. Upon comparative analysis, it can be observed that the displacement of points B and D in x-direction is equivalent, as is the displacement of points A and C in the same direction, which suggests that during the process of un- and folding the roof, these two sets of points always remain coplanar with the scissor joint units, ensuring coordinated motion of the structure. As the entire structure unfolds, the displacement of all reference points in x-direction exhibits a smooth and gradual increase, reaching its peak value at t = 10 s. The panel comprising points O, B, and D rotates around the x-axis and y-axis, resulting in a relatively minor overall displacement in the y-direction for point D, which is only 182.33 mm. Moreover, the displacement in z-direction of point D showcases the gradual decrease in the overall height of the structure as it unfolds.

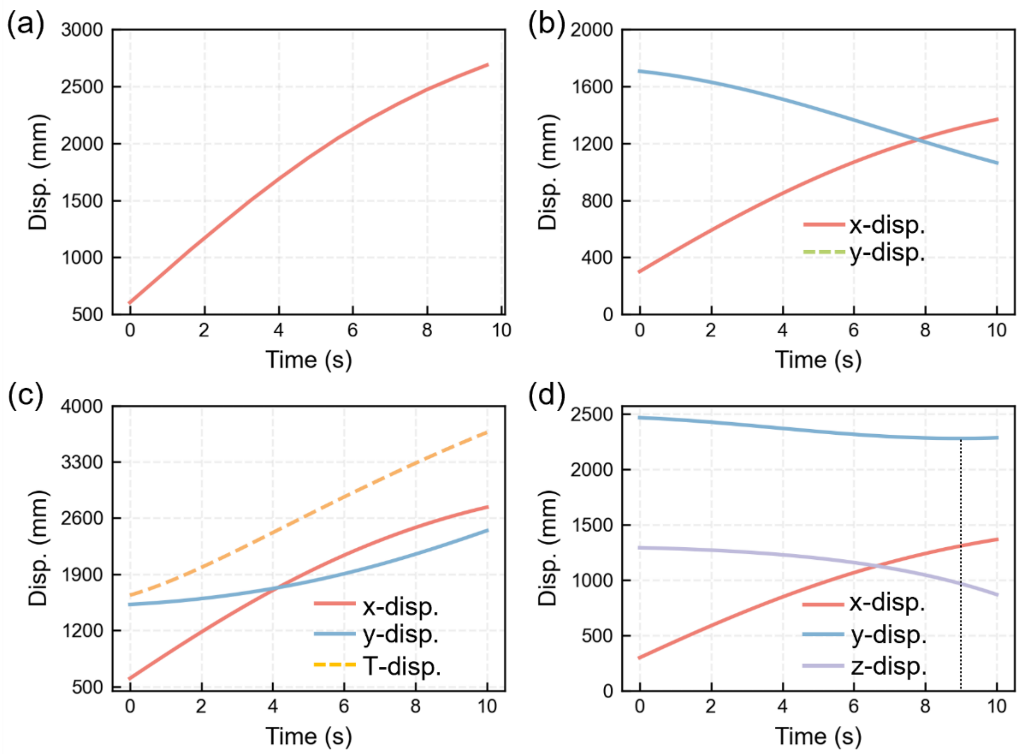

Fig. 8 The displacement-time curves of the Miura-ori retractable roof. (a), (b), (c), and (d) denote the displacement-time relationship of points A, B, C, and D, respectively. (x-, y-, and z-disp. represent the displacement components of a reference point in the three principal axis directions while T-disp. is the total displacement of the corresponding point.)

Fig. 9 depicts the velocity-displacement curves of points A, B, C, and D. The upper roof comprises four identical parallelograms, resulting in comparable velocities of points A and C, as well as B and D, at the onset of the motion. Specifically, the velocity of points A and B is roughly twice that of C and D (more vividly demonstrated in Fig. 9e). For a significant period, the velocity of point C in x-direction consistently exceeds that in y-direction, although the disparity between the two gradually diminishes. At t = 8.36 s, the x- and y-direction of the velocity at point C are both 140.80 mm/s.

Subsequently, the y-direction of the velocity at point C overtakes the x-direction. This indicates that, during the motion process, the structure initially moves predominantly in x-direction and gradually shifts towards movement in y-direction. The velocity of point D, as depicted in Fig. 9e, gradually decreases over time, reaching a minimum value of 102.68 mm/s at t = 7.76 s. Afterward, it gradually increases and eventually surpasses the velocities of points A and B.

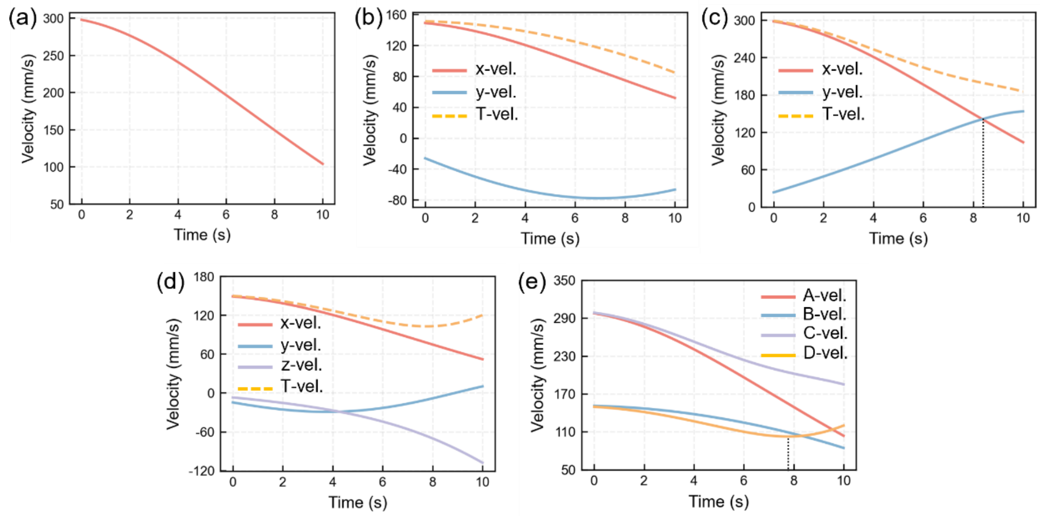

Fig. 9 The velocity-time curves of the Miura-ori retractable roof. (a), (b), (c), and (d) denote the velocity-time relationship of points A, B, C, and D, respectively; (e) depicts the velocity comparison of four reference points. (x-, y-, and z-vel. represent the velocity components of a reference point in the three principal axis directions while T-vel. is the total velocity of the corresponding point.)

4.2 The arched variation of retractable roof

The arched variant retractable roof model, as shown in Fig. 10, comprises three arched scissor-jointed mechanisms, consisting of six basic origami units. The length of each bar in the lower scissor joint unit measures 2100 mm (2c). To ensure smooth and uninterrupted movement of the entire structure, we have set the angles between the retractable panels to be $\xi_1 = 45°$ and $\xi_2 = 180°$, corresponding to the fully un- and folded states of the arched variant of the retractable roof. For further details regarding the specific parameters of the retractable roof model, kindly refer to Table 2.

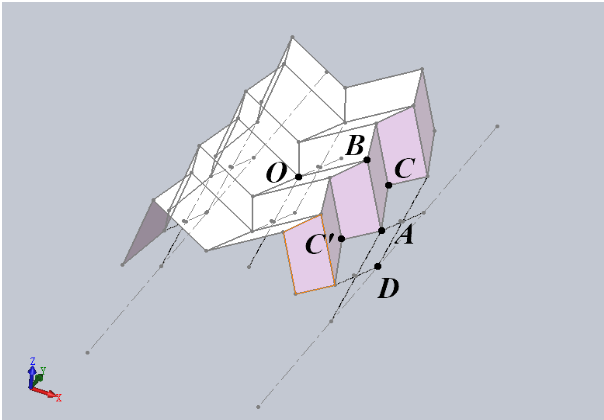

Fig. 10 The Arched variation of the Miura-ori retractable roof model.

Table 2 The specific parameters of the arched variation of Miura-ori retractable roof

a **(mm)**	***h*** **(mm)**	β_1 **(°)**	β_2 **(°)**	ξ_1 **(°)**	ξ_2 **(°)**	***c*** **(mm)**
1500	1000	80	70	45	180	1050

Note: the parameters are illustrated in Fig. 4 and Fig. A. 1.

We utilize revolute connections in SolidWorks to link the bars of the transverse and longitudinal scissor joint units. Through path coordination, the retractable roof moves along a predetermined motion trajectory line (the dash lines in Fig. 10) and is propelled by a motor. A rotational driving motor is positioned at point O, the center point of the entire structure (as depicted in Fig. 10). This motor uniformly increases the included angle between adjacent roof panels at an angular velocity of 9 °/s and for 15 seconds. The simulation, presented in Fig. 11, demonstrates that the entire mechanism can smoothly achieve opening and closing.

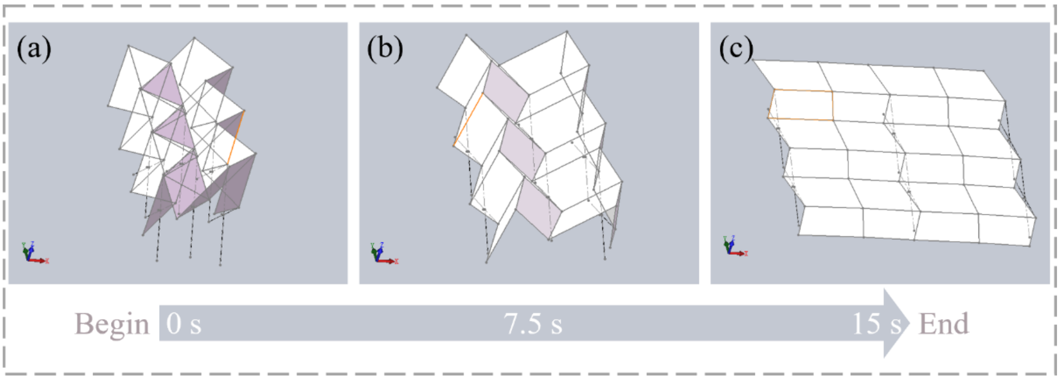

Fig. 11 The motion of the arched variation of the Miura-ori retractable roof. (a), (b), and (c) respectively denote the 0th, 5th, and 15th seconds during the course of motion.

Fig. 12 illustrates the displacement-time curves of reference points A, B, C, and D concerning the center point O of the structure. As the structure is in motion, the displacement of all reference points in x-direction increases smoothly and attains their maximum values at $t = 15$ s. Point B follows circular motion around the center point O in y-direction, with its displacement in this direction gradually decreasing over time. Point D represents the intersection of the lower ends of two scissor joint units and experiences no displacement in y-direction. Nevertheless, its displacement in z-direction gradually increases (i.e., moving upward) over time, then begins to decrease slowly at $t = 7.40$ s, before moving upward again at $t = 10.96$ s. Notably, during the period of $t = 7.40 \sim 10.96$ s, the structure primarily unfolds in x-direction, with a relatively minor degree of unfolding in y-direction. Point D ultimately reaches its highest point at -640.31 mm. Simultaneously, the displacements of points C and C' in x-direction remain precisely the same, indicating that the entire structure moves in a coordinated manner.

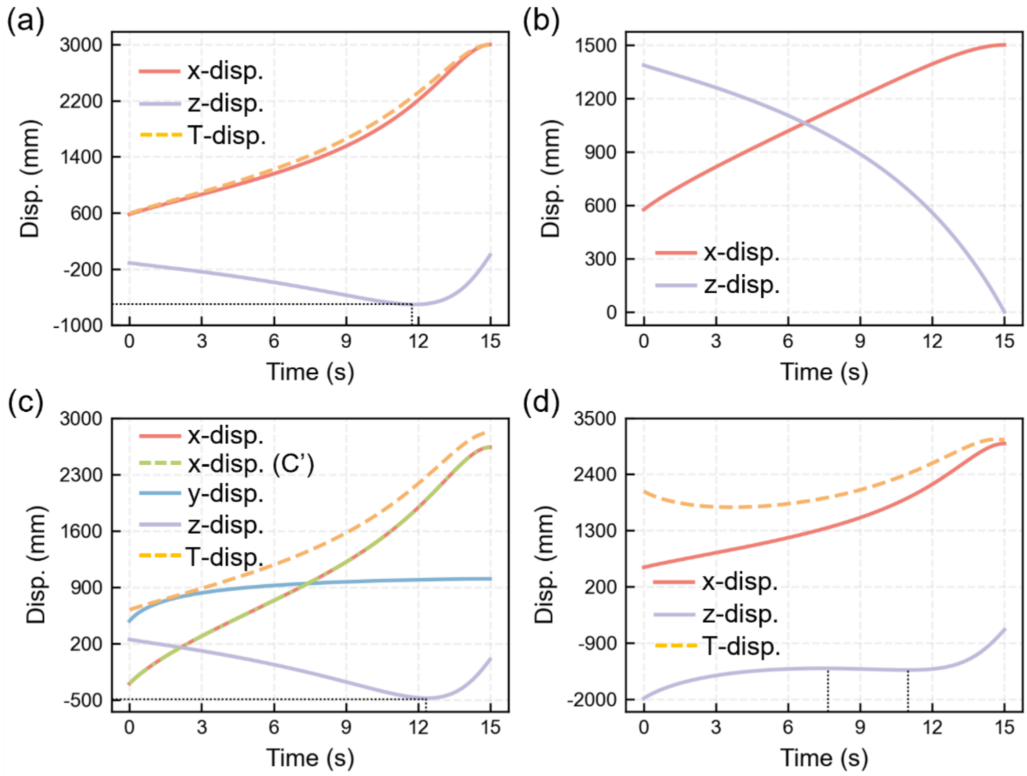

Fig. 12 The displacement-time curves of the arched variation of retractable roof. (a), (b), (c), and (d) denote the displacement-time relationship of points A, B, C, and D, respectively. (x-, y-, and z-disp. represent the displacement components of a reference point in the three principal axis directions while T-disp. is the total displacement of the corresponding point.)

The velocity-displacement curves of the key reference points, as shown in Fig. 13, reveal that the motion process can be segmented into three stages. During the initial stage (t = 0~4.76 s), the velocity components of each reference point in all directions are relatively uniform. In the middle stage (t = 4.76~13.20 s), the total velocity and x-component velocity of the four reference points are nearly equivalent, indicating that the movement is primarily in x-direction. In the subsequent stage (t = 13.20~15.0 s), the x-component velocities of points A, C, and D decrease rapidly to zero, demonstrating that they move primarily in the z-direction. In contrast, point B undergoes circular motion around the center point O, with a relatively lower velocity compared to other points but with a smooth movement.

Points C and D exhibit a significant decrease in velocity, followed by a rapid increase, with the times of minimum velocity being identical at t = 4.96 s and t = 4.76 s, respectively. In the early stage, points A and B experience similar velocity changes, with a substantial reduction in velocity during the initial stage (at t = 2.0 s and t = 3.4 s, respectively). The decrease in velocity for point A is more significant than that of point B. Throughout the motion process, the velocity of point B remains the lowest among the four key reference points. During the period of t = 0 to 4.12 s, v_D is greater than v_A, but the difference gradually decreases, and at t = 4.12 s, the instantaneous velocities of these two points are the same. Subsequently, their velocities become closer and exceed the velocity of point C at t = 11.68 s.

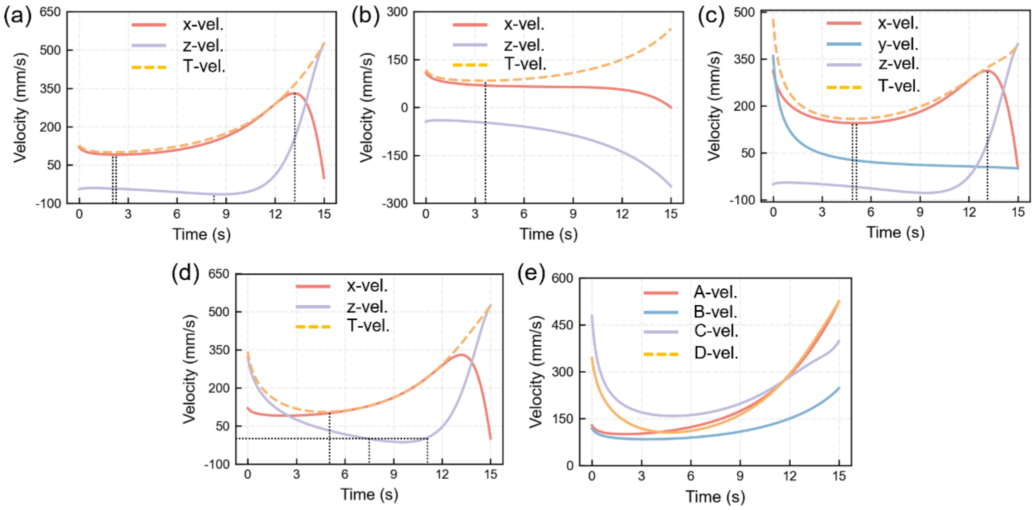

Fig. 13 The velocity-time curves of the arched variation of the Miura-ori retractable roof. (a), (b), (c), and (d) denote the velocity-time relationship of points A, B, C, and

D, respectively; (e) depicts the velocity comparison of four reference points. (x-, y-, and z-vel. represent the velocity components of a reference point in the three principal axis directions while T-vel. is the total velocity of the corresponding point.)

4.3 Fan-shaped variant of retractable roof

The fan-shaped variant retractable roof model (depicted in Fig. 14) comprises four basic units, with two units oriented in the circumferential and radial directions, respectively, and the length of the bars in the lower scissor joint units is l = 4500 mm. To ensure smooth movement of the entire structure, the angles between the retractable roof panels are θ_1 = 30° and θ_2 = 180° for the fully folded and unfolded states of the fan-shaped variant, respectively. For additional information regarding the specific parameters of the retractable roof model, kindly refer to Table 3.

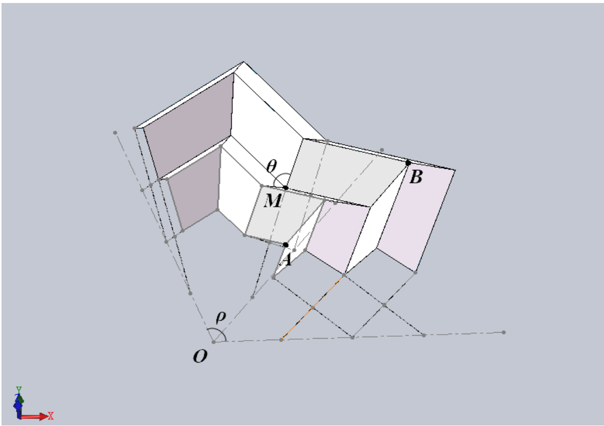

Fig. 14 The fan-shaped variation of the Miura-ori retractable roof model.

Table 3 The specific parameters of the fan-shaped variation of the Miura-ori retractable roof

b_1 (mm)	a_c (mm)	φ_1 (°)	φ_2 (°)	θ_1 (°)	θ_2 (°)	l (mm)
1500	2000	80	60	30	180	4500

Note: the parameters are illustrated in Fig. A. 2.

The simulation software employs revolute connections to link the bars of the transverse and longitudinal scissor joint units at the connection points. By path coordination, the retractable roof moves along the trajectory line at the lower end of the scissor joint units (the dash lines in Fig. 14) and is driven by a motor. In Fig. 14, a rotational driving motor is installed at point M, which denotes the center point of the upper panel structure. This motor uniformly increases the angle between two adjacent panels at an angular velocity of 10°/s and persists for 15 seconds. The simulation, presented in Fig. 15, illustrates that the entire mechanism achieves smooth opening and closing.

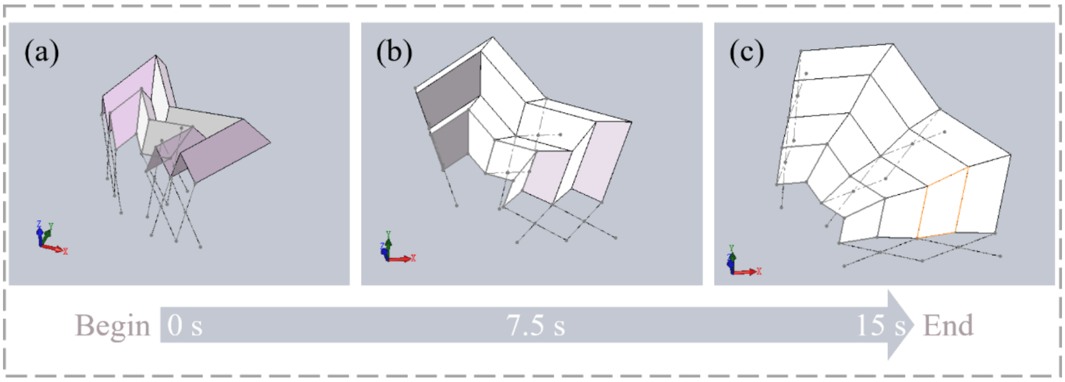

Fig. 15 The motion process of the fan-shaped variation of the Miura-ori retractable roof.

The displacement-time curves of the motion reference points A and B during the movement process are shown in Fig. 16a-b. The displacements of the retractable roof in y-direction undergo minimal change, with a displacement increase of only 6.68% as the roof unfolds. During the motion process, point A follows a counterclockwise path around the center point O, with its displacement in x-direction gradually decreasing as time *t* increases. Since point B shares the same polar angle as point A in the projection plane, their displacements and velocities are identical in y-direction, as evident from the trend of the curves in Fig. 16b. Nevertheless, due to the outward expansion movement of the retractable roof, the displacement of point B exhibits an opposite trend to that of point A in x-direction. As the motion of the retractable roof continues, the displacement of point B in x-direction gradually increases, but the rate of displacement change remains comparable to that of point A. The displacement of point B in z-direction reflects the variation pattern of the height of the retractable roof, which decreases gradually with time t during the unfolding process, exhibiting a relatively minor rate of change, and its curve is approximately linear.

Fig. 16c presents the curve of the distance (polar radius) from point A to the polar axis in the projection plane as a function of time. The polar radius of point A increases from an initial value of 2678.54 mm to 4313.43 mm, and its rate of change gradually decreases, which indicates that during the unfolding process, the inner edge of the fan-shaped variant roof panel gradually moves away from the center of the structure, and the space in the middle increases as the structure unfolds. Fig. 16d depicts the variation of the maximum angle ρ (as shown in Fig. 14) of the structure. The ρ gradually decreases with time t, with its rate of change also gradually decreasing. Throughout the unfolding process, the angle ρ decreases from 124.57° to 80.15°, representing an opening efficiency of 35.66% in the circumferential direction. Overall, the movement of the entire structure is well-coordinated.

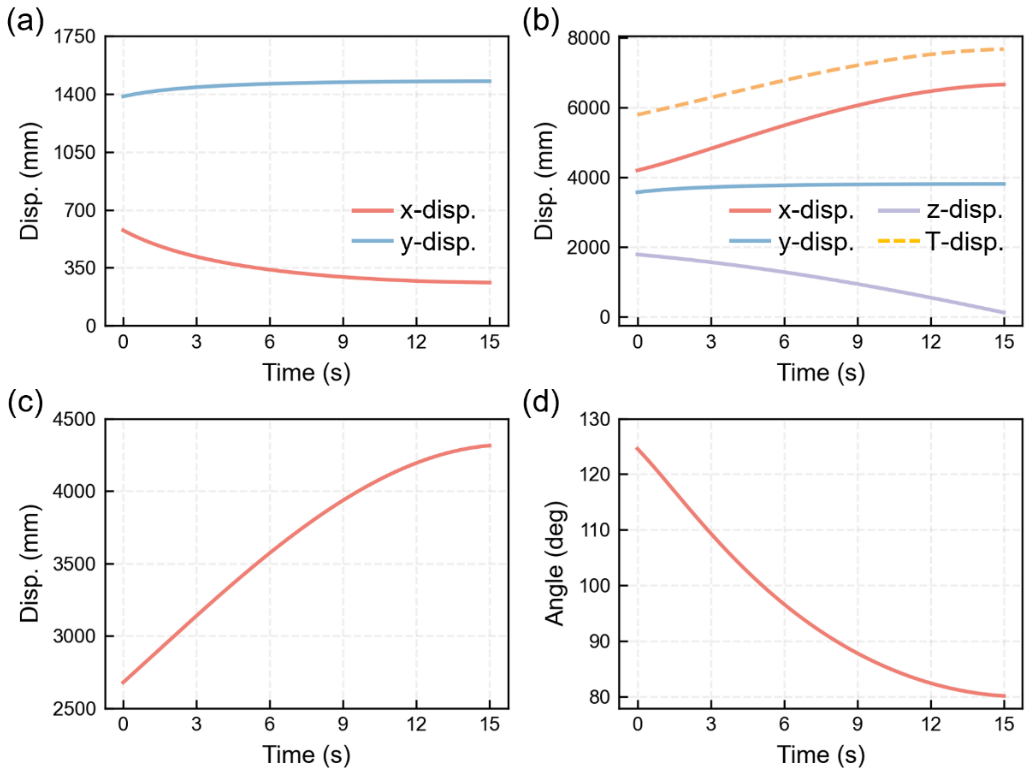

Fig. 16 Parameters at each reference point of the fan-shaped variant retractable roof. (a) and (b) denote the displacement-time relationship of points A and B, respectively; (c) depicts the distance of point A from the polar; (d) is the maximum angle ρ of the retractable roof. (x-, y-, and z-disp. represent the displacement components of a reference point in the three principal axis directions while T-disp. is the total displacement of the corresponding point.)

5. Conclusion

Three different retractable roof structure systems, inspired by the concept of origami, are proposed in this paper, and the process of conducting thick plate analysis and parametric modeling, adopting Grasshopper, is elaborately described. Theoretical analysis of the three retractable roof structures is then carried out using geometric formulas, followed by a detailed motion simulation analysis. Our main contributions and conclusions:

(1) Three novel retractable roof structure systems are proposed. We propose three new types of retractable roof structure systems by combining the geometric principles of the Miura-ori mechanism and its arched and fan-shaped variations with the scissor hinge rectangular unit. The necessary conditions for the coordinated motion of the three new retractable roof structure systems in two directions are further derived, and the compatibility solution is proposed for cases where coordinated motion cannot be achieved between the scissor joint and origami mechanisms.

(2) The effect of thickening on the maximum opening ratio of the structure is presented. The thickening method based on the shape adjustment technique is proposed, and the formula for the maximum opening ratio of the new retractable roof system is derived accordingly. The analysis results demonstrate that the effect of panel thickness on the maximum opening ratio shows different patterns as the value of the notch length varies. Specifically, as the depth of the cut increases while keeping the panel thickness constant, the maximum opening ratio also increases. When it comes to the case where the panel thickness is fixed and the depth of the cut varies, a consistent pattern is observed: the maximum opening ratio increase as the length of the notch enlarges.

(3) Parametric modeling steps are elaborately described. The rigid origami truss structure, based on the principles of origami mechanism, is established by adopting a “two-step” approach that uses Grasshopper and isogeometric segmentation). The modeling steps and parameter control methods are described in exhaustive detail.

(4) The kinematic patterns of the new retractable roof structures are investigated. The simulation demonstrates that all three types of structures can be un- and folded smoothly without any occurrence of motion interference: 1) During the motion process of the Miura-ori retractable roof structure, the primary movement is transverse, which gradually shifts to longitudinal movement. It is sufficient to control the movement during the initial phase of motion as the speed of motion slows down in the later stages. 2) As to the arched variant, the velocity relationship between the four key reference points is such that $v_A \approx v_D > v_C > v_B$, which suggests that the overall motion speed of the edge ends and scissor joint units is greater than that of the middle part of the structure. Therefore, in practical applications, it is crucial to prioritize control of the speed of the far end. 3) As the fan-shaped variant retractable roof structure unfolds, the z-component of point B reflects a nearly constant rate decrease in the structure height. Additionally, the included angle ρ of the structure gradually decreases with increasing time t, with a progressively slowing rate of decrease.

We, in this paper, primarily focus on the development of new structural systems and the theoretical analysis and motion simulation of their coordinated motions. The following aspects, nevertheless, require further research. Firstly, there is still much exploration needed for retractable roof structure systems that draw inspiration from origami while also incorporating more practical designs. Moreover, future research is recommended to concentrate on refining the design of the nodes and examining their impact on the structural motion and mechanical performance, for we streamlined the design of connection nodes in the current study. Lastly, it is of utmost importance to carry out practical experiments to verify the workability of the structures and the precision of the theoretical investigations, owing to the cross-disciplinary nature of this research.

Declaration of competition interest

All authors have no conflict of interest to declare.

Acknowledgment

This work was supported by the National Natural Science Foun- dation of China (Grant no. 51778129), High Level Talent Projects of Six Talent Peaks in Jiangsu Province, China (Grant no. JZ-010), Young Academic Leaders of Qing Lan Fund Project of the Jiangsu Higher Education Institutions of China.

References

[1] Lang R, Nemec I, Martinasek J. Specific aspects of tensile structures. Appl Mech Mater 2015;769:19–24.

[2] Kassabian PE, Zhong Y, Pellegrino S, Civ L. Retractable roof structures. Struct Build 1999;134:45–56.

[3] Pérez-Valcárcel J, Muñoz-Vidal M, Suárez-Riestra F, López-César IR, Freire-Tellado MJ. A new system of deployable structures with reciprocal linkages for emergency buildings. J Build Eng 2021;33:101609.

[4] Pawlak-Jakubowska A, Romaniak K. Kinematics of the retractable roofing module constructed from three roof panels. J Build Eng 2021;38:102169.

[5] Fuller RB. Synergetics: Explorations in the geometry of thinking. California: Estate of R. Buckminster Fuller; 1982.

[6] Fuller RB. Operating Manual for Spaceship Earth. Lars Müller Publishers; 2008.

[7] Lu D, FuLing G. Shape-sizing nested optimization of deployable structures using SQP. J Cent South Univ 2014;21:2915–20.
[8] Hoberman C. Radial expansion/retraction truss structures. US5024031A, 1991.
[9] You Z, Pellegrino S. Foldable bar structures. Int J Solids Struct 1997;34:1825–47.
[10] You Z, Pellegrino S. Cable-stiffened pantographic deployable structures part 2: mesh reflector. AIAA J 1997;35:1348–55.
[11] Wujun C, Gongyi F, Jinghai G, Yanli H, Shilin D. A new design conception for large span deployable flat grid structures. Int J Space Struct 2002;17:293–9.
[12] Jianguo C. Shape and stress analysesand moving process researchof new types of deployablestructuters. Ph.D. Southeast University, 2012.
[13] Zhang Q, Jia W, Lee DS, Cai J, Feng J. Inverse design of planar morphing scissor structures with end constraints. Struct Multidiscip Optim 2022;65:70.
[14] Li Y, Krishnan S. Geometric design and optimization of scissor-type deployable structures. J Build Eng 2023;65:105724.
[15] Smith CW, De Focatiis DSA, Guest SD. Deployable membranes designed from folding tree leaves. Philos Trans R Soc Lond Ser Math Phys Eng Sci 2002;360:227–38.
[16] Lang RJ, Magleby S, Howell L. Single degree-of-freedom rigidly foldable cut origami flashers. J Mech Robot 2016;8:031005.
[17] Miura K. Method of packaging and deployment of large membranes in space. Inst Space Astronaut Sci Rep 1985;618:1–9.
[18] Miura K. Folded map and atlas design based on the geometric principle. Proc. 20th Int. Cartogr. Conf., Beijing, China: 2001.
[19] Karni E, Pellegrino S. A retractable small-span roof based on thin-walled lightweight spatial units. Int J Space Struct 2007;22:93–106.
[20] Tonon OL. Geometry of spatial folded forms. Int J Space Struct 1991;6:227–40.
[21] Kahramanoğlu B, Çakıcı Alp N. Enhancing visual comfort with Miura-ori-based responsive facade model. J Build Eng 2023;69:106241.

[22]Gattas JM, Wu W, You Z. Miura base rigid origami: parameterizations of first level derivative and piecewise geometries. J Mech Des 2013;135:111011.

[23]Xiang XM, Lu G, Ruan D, You Z, Zolghadr M. Large deformation of an arc-Miura structure under quasi-static load. Compos Struct 2017;182:209–22.

[24]Zhang Q, Wang X, Lee DS, Cai J, Ren Z, Feng J. Development of kinetic origami canopy using Arc Miura folding patterns. J Build Eng 2021;43:103116.

[25]Fulong J. Study on curved surface modeling based on Miura-ori. Master. Nanjing University, 2018.

[26]Waldron. Kinematics, dynamics and design of machinery. 2nd ed. Wiley India Pvt. Limited; 2007.

[27]Smart WM. Textbook on spherical astronomy. Cambridge, New York: Cambridge University Press; 1977.

[28]Uicker JJ, Pennock GR, Shigley JE. Theory of machines and mechanisms. Oxford, U.K.: Oxford University Press; 2011.

[29]Liao Y, Krishnan S. Geometric design and kinematics of spatial deployable structures using tripod-scissor units. Structures 2022;38:323–39.

[30]Alegria Mira L, Thrall AP, De Temmerman N. Deployable scissor arch for transitional shelters. Autom Constr 2014;43:123–31.

[31]Tachi T. Simulation of rigid origami. Origami 4, Massachusetts, United States: A K Peters/CRC Press; 2009.

[32]Chen Y, Peng R, You Z. Origami of thick panels. Science 2015;349:396–400.

[33]Huang L, Zeng P, Yin L, Liu B, Yang Y, Huang J. Design and kinematic analysis of a rigid-origami-based underwater sampler with deploying-encircling motion. Mech Mach Theory 2022;174:104886.

[34]Nelson TG, Avila A, Howell LL, Herder JL, Machekposhti DF. Origami-inspired sacrificial joints for folding compliant mechanisms. Mech Mach Theory 2019;140:194–210.

[35]Huffman DA. Curvature and creases: a primer on paper. IEEE Trans Comput

1976;25:1010–9.

[36]Edmondson BJ, Lang RJ, Magleby SP, Howell LL. An offset panel technique for thick rigidily foldable origami, New York, United States: American Society of Mechanical Engineers Digital Collection; 2015.

[37]Lv C, Krishnaraju D, Konjevod G, Yu H, Jiang H. Origami based mechanical metamaterials. Sci Rep 2014;4:5979.

[38]Yunlong H. Design and analysis offoldable plate structures. Master. Southeast University, 2011.

Appendix A.

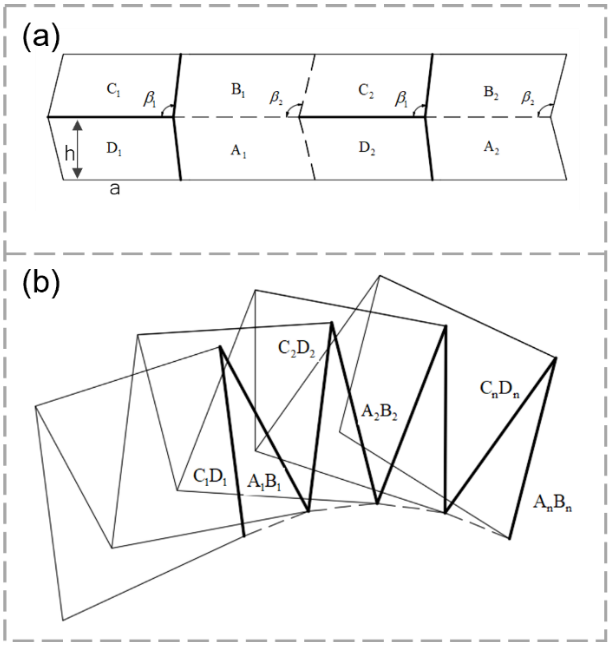

Fig. A. 1 Geometric parameters of the arched variant. (a) the arched variant unit; (b) The arched variant unit after folding.

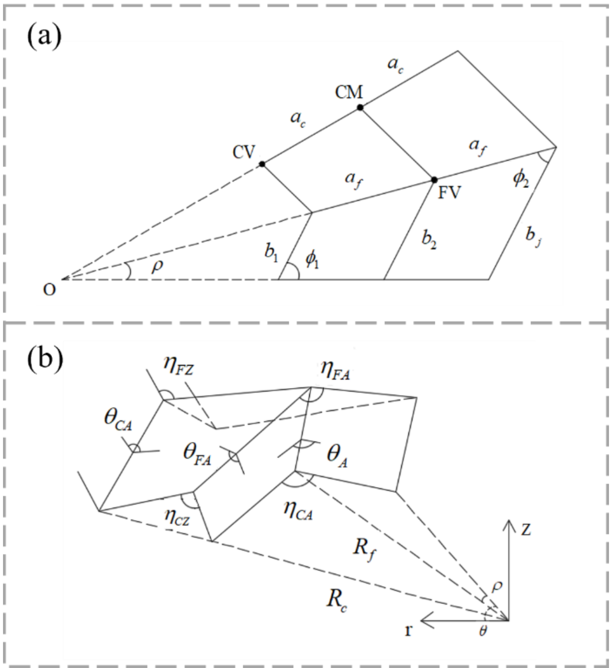

Fig. A. 2 Geometric parameters of the fan-shaped variant. (a) The fan-shaped variant unit; (b) The fan-shaped variant unit after folding.

Appendix B. Derivation of the equation for thick plate

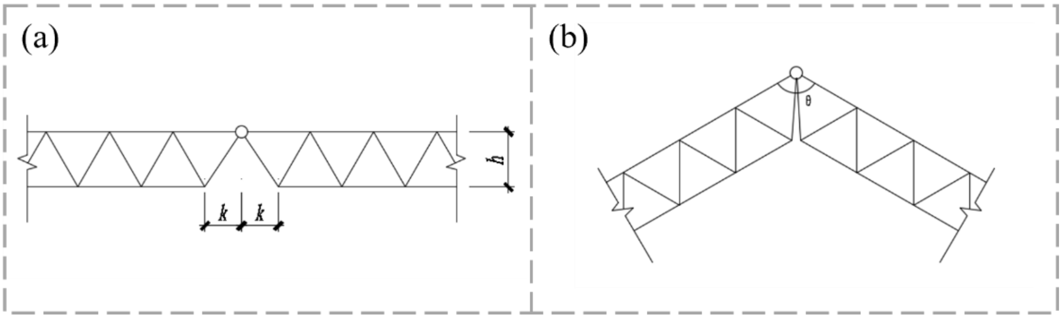

Fig. B. 1 The simplified diagram of the thick plate analysis. (a) Unfolded state; (b) Folded state.

The simplified diagram of the thick plate analysis, illustrated in Fig. B. 1, involves cutting the panels on both sides of the crease with a thickness of h to create symmetrical notches with a length defined as k. The fold angle, θ, is defined as the angle between adjacent panels. The minimum value of $\theta_{\min}$, when the panels are fully folded, is related to both h and k. The relationship between these three can be expressed as:

$$\theta_{\min} = 2\arctan\frac{h}{k} \tag{B.1}$$

To control the maximum opening rate of the Retractable roof structure designed with origami principles, the values of h and k (related to plane thickness and notch length) require to be analyzed and studied. The formula of the opening rate is

$$\eta = 1 - \frac{S_O}{S_C} \tag{B.2}$$

where S_O and S_C are the areas of the retractable roof when fully open and closed, respectively. S_O represents the projection area of the retractable roof when the origami mechanism is wholly folded, while S_C denotes the projection area when it is totally unfolded. For a Miura-ori retractable roof with n_1 and n_2 units in the longitudinal (y) and transverse (x) directions, respectively, if the acute angle of the parallelogram unit is β and its corresponding sides lengths are a and b, respectively, then expressions for S_O and S_C can be obtained accordingly:

$$S_C = n_1 \cdot n_2 \cdot (4ab\cos(\frac{\pi}{2} - \beta)) = 4abn_1n_2 \sin\beta \tag{B.3}$$

$$S_O = n_1 \cdot n_2 \cdot (4ab\cos(\frac{\pi}{2} - \beta) \cdot \sin\frac{\theta_{\min}}{2}) = 4abn_1n_2 \sin\beta \sin\frac{\theta_{\min}}{2} \tag{B.4}$$

By substituting Eq. (B.1), Eq. (B.3), and Eq. (B.4) into Eq. (B.2), Eq. (B.5) can be obtained.

$$\eta = 1 - \frac{S_O}{S_C} = 1 - \frac{4abn_1n_2 \sin\beta \sin\frac{\theta_{\min}}{2}}{4abn_1n_2 \sin\beta} = 1 - \sin\frac{\theta_{\min}}{2} = 1 - \sin(\arctan\frac{h}{k}) \tag{B.5}$$

Appendix C. Parametric modeling procedure for the retractable roof structure

The Grasshopper modeling process can be broadly classified into two parts. In this study, we demonstrate the parameterization of the retractable roof model using the classic Miura-ori as an example.

(1) Modeling of zero-thickness origami mechanism

To determine the shape of the retractable roof panel in various states, a basic Miura-ori structure is established, without considering the influence of thickness, members, and other factors.

Step 1: Construct the motion trajectory and label the vertices.

By defining the side lengths a and b of a parallelogram using coordinates and utilizing the “Arc” command, the vertices movement paths of the parallelogram throughout its entire deployment process can be constructed. The “Construct Domain” command allows for the control of the position of vertex A at any given time on its movement path, as shown in the figure below.

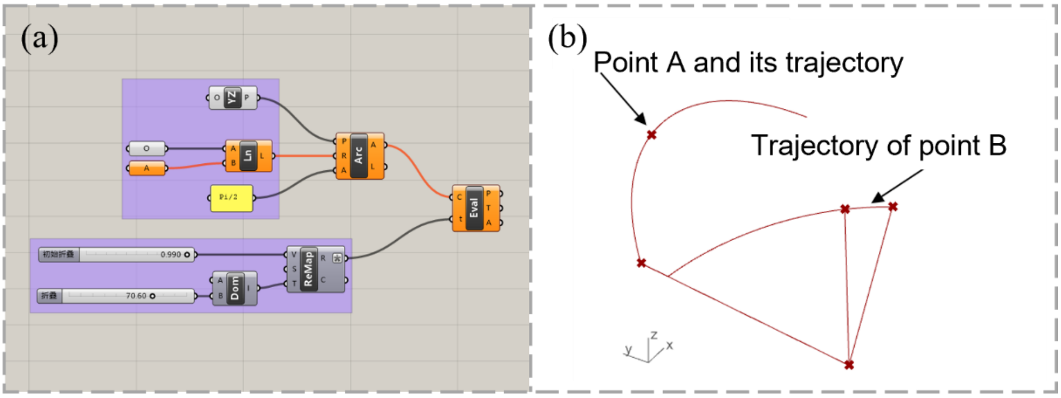

Fig. C. 1 Construct the motion trajectory and label the vertices. (a) Grasshopper command; (b) Corresponding graphics in Rhino.

Step 2: Create a single degree of freedom connection point.

Create a reference sphere with a center at point A using the “Sphere” command, and then use “Brep/Curve” command to automatically calculate the intersection points between the reference sphere and the motion path to ensure that the position of point A always determines the position of point B. All vertices are related to point A, and the entire structure has, therefore, a single degree of freedom.

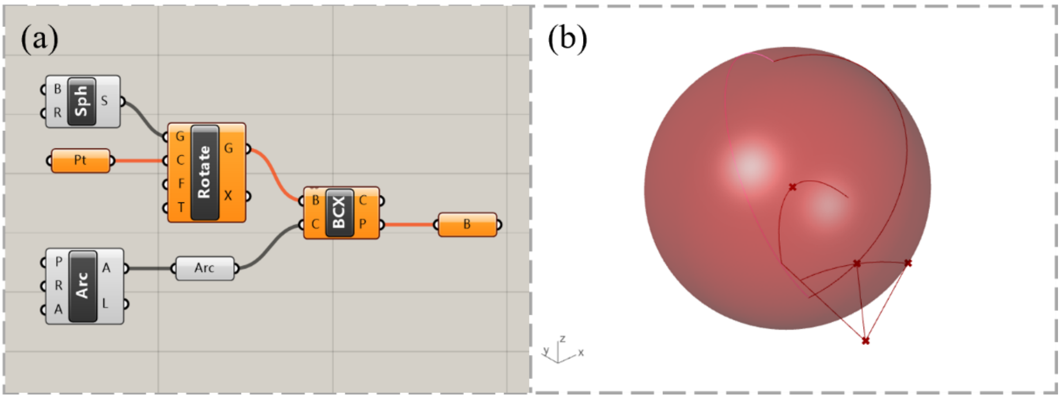

Fig. C. 2 Create a single degree of freedom connection point. (a) Grasshopper command; (b) Corresponding graphics in Rhino.

Step 3: Build the zero-thickness panel.

By utilizing vector displacement and mirroring commands on the key points A and B identified in the previous steps, a parallelogram panel with controllable position and orientation is formed, which further forms a set of panel units with adjustable parameters. Lastly, all panel units, using the “Brep Join” command, are integrated into a single entity, as illustrated in. The entire mechanism can achieve a single degree of freedom un- and folding using the “Construct Domain” progress bar introduced in step 1.

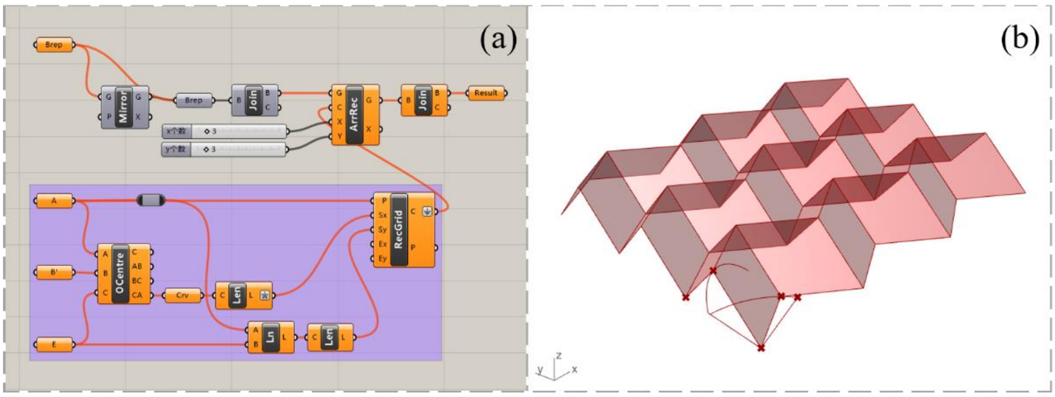

Fig. C. 3 Build the zero-thickness panel. (a) Grasshopper command; (b) Corresponding graphics in Rhino.

(2) Establishing retractable roof grid structure with thickness.

A planar truss structure with thickness, based on the previously built zero-thickness panel element, is constructed to establish a retractable roof structure suitable for practical analysis.

Step 1: Divide the panel to get the meshes.

To begin, set the number of mesh lines along the u- and v-direction of the single roof panel to the corresponding numbers. Next, divide the panel into several small parallelogram meshes along the u- and v-direction using the “Divide Domain” command. The center points of each small mesh are then extracted using the "Area" and "Srf CP" commands.

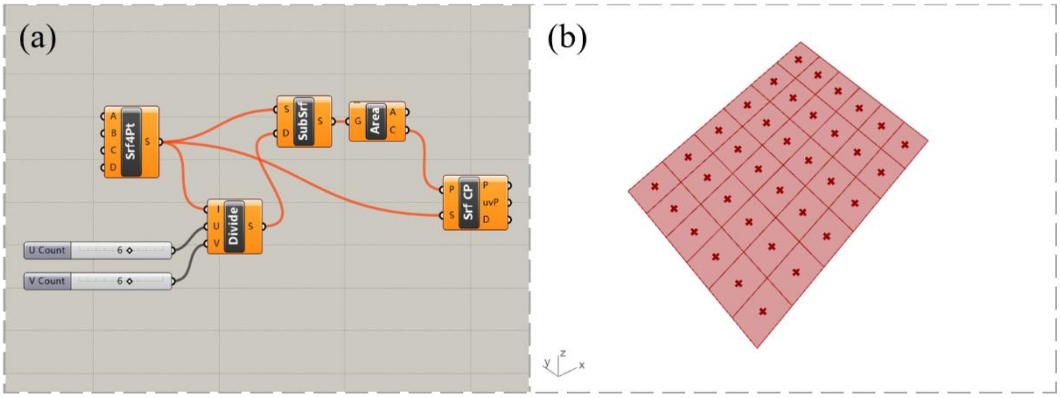

Fig. C. 4 Divide the panel to get the mesh. (a) Grasshopper command; (b) Corresponding graphics in Rhino.

Step 2: Construct single-piece trusses.

The normal direction of each mesh plane is determined using the "Eval Srf" command. The center points of meshes, extracted from step 1, are then offset a certain distance, along the normal direction, which is set as the thickness of the truss structure. The "Graft Tree" and "Flip" commands are then used to adjust the coding of each point based on the characteristics of the mesh distribution of the truss structure. The upper and lower chords, as well as the web members, are subsequently connected according to different coding arrangements. Finally, the "Joint Curves" command is used to join them together to form a complete truss structure.

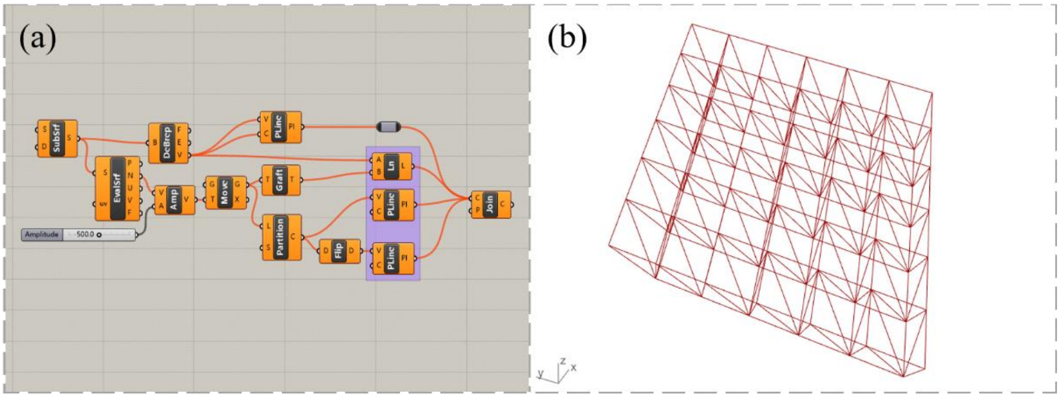

Fig. C. 5 Construct single-piece trusses. (a) Grasshopper command; (b) Corresponding graphics in Rhino.

Step 3: Create a retractable roof structure with rigid folding capability.

Several single truss structures are integrated to form a retractable roof structure with rigid folding capability based on the number and position of the previously described zero-thickness folding panels. To achieve retractable roof structures with varying heights, shapes, and folding states, one can simply adjust the corresponding parameter values in the key steps outlined above.

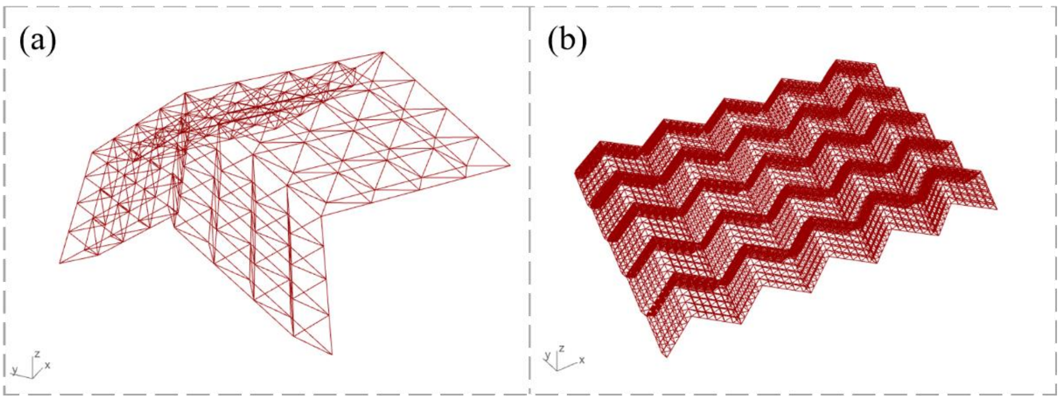

Fig. C. 6 Create a retractable roof structure with rigid folding capability: (a) Grasshopper command; (b) Corresponding graphics in Rhino.